ISSN 1023-1935, Russian Journal of Electrochemistry, 2020, Vol. 56, No. 10, pp. 795–808. © Pleiades Publishing, Ltd., 2020.
Published in Russian in Elektrokhimiya, 2020, Vol. 56, No. 10, pp. 880–895.

New Perspectives on Turbulence[1]

John Newman*

Department of Chemical and Biomolecular Engineering University of California, Berkeley, California, 94720-1462 USA
**e-mail: newman@newman.cchem.berkeley.edu*

Received September 28, 2019; revised November 6, 2019; accepted February 20, 2020

Abstract—Recent work on the dissipation theorem of turbulent flow is reviewed, with examples in rotating cylinders, pipe flow, and flow past a flat plate at zero incidence. The dependence of the eddy viscosity and eddy diffusivity on distance from a solid wall is reviewed and is supported by treatment of fluctuations. The role of the viscous sublayer in fluid friction is discussed.

Keywords: eddy viscosity, eddy diffusivity, dissipation theorem, viscous sublayer, fluctuations
DOI: 10.1134/S1023193520100092

Between 1940 and about 1980 there was an outpouring of new work on turbulence in the Russian scientific literature. It is appropriate that a special issue honoring the 100th birthday of V. S. Bagotsky should include a discussion of turbulence, which is of great interest in electrochemistry. Electrochemical systems are great for investigating turbulence and for showing how system behavior is affected by turbulence.

The focus of electrochemists is on the interface and how reactions occur at an electrode. Mass-transfer limitations are a complicating feature which must be accounted for to get the correct interpretation of the chemical phenomena. But turbulence is a complex phenomenon which has defied the efforts of physicists to clarify it and to develop a firm predictive theory. The work here started with trying to understand very good mass-transfer data in an electrochemical system comprised of a stationary outer cylindrical electrode and an inner rotating electrode. Some effort was devoted here to demonstrating how the results depend on κ, the ratio of the inner radius to the outer radius and the development of the dissipation theorem of turbulence.

This theory attempts to find local laws governing the relationships among various statistical averages of turbulence, principally between the eddy viscosity and the volumetric dissipation. This gives some understanding for the rotating-cylinder system, but it really progresses when it is applied to steady fully developed flow in a circular pipe. A 1932 paper by Nikuradse [1] describes extensive measurements of velocity profiles, friction factors, and eddy viscosities for Reynolds numbers from 4000 to 3.2 million. The dissipation theorem explains the results but also derives much information from this very early but meticulous study.

The dissipation theorem is also applied to the developing flow past a flat plate at zero incidence, where the flow is laminar (and understood) near the leading edge but then passes through a transition to turbulence and eventually to fully developed turbulence somewhat like what Nikuradse finds for pipe flow as the Reynolds number varies.

The rotating disk is a convenient experimental system used widely in electrochemical studies. The fluid flow in this system is also well studied, showing laminar flow near the axis of rotation, followed by a transition region, and eventually an outer region of fully developed turbulence. This is quite similar to what is found with the flat-plate system, with different regions occurring as the flow moves over the surface.

It remains to be seen how well the dissipation theorem holds up under continued scrutiny.

In a somewhat parallel development, Kolmogorov [2] develops a theory of the decay of turbulence in a system where the medium is nearly homogeneous and isotropic. This should have a relationship to the decay of dissipation in other geometries.

In separate but related studies, it becomes clear that the turbulent shear flow has a region very near the wall where the level of turbulence declines gradually as the wall is approached [3–5]. This is termed the viscous sublayer. Since it is so close to the surface, electrolytic mass transfer at high Schmidt numbers ($Sc = \nu/\mathscr{D}$, the ratio of the kinematic viscosity to the diffusion coefficient) is a preferred means of investigation.

A surprising result of the dissipation theorem of turbulence is that the friction is very strong in this layer and that a large amount of the overall friction is explained by the viscous sublayer. This shows up in the

[1] In memory of the famous electrochemist Vladimir Sergeevich Bagotzky whose centenary is celebrated in 2020.

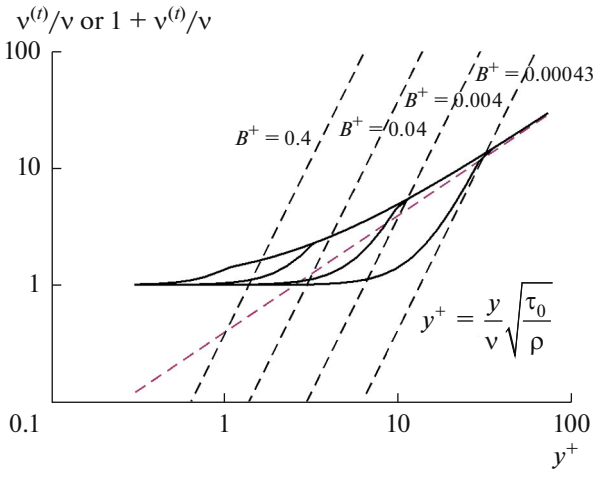

Fig. 1. Eddy viscosity versus distance. The wall stress τ_0 is a common way to generate a universal profile near a wall, using the coordinate y^+. Three straight lines (on a log–log plot) are the components of the total viscosity. The first component is the kinematic viscosity itself, which here is a horizontal line at a value of 1. In the viscous sublayer, the eddy viscosity can be represented by a slope of 3, as in $\nu^{(t)}/\nu = B^+(y^+)^3$. Just outside the viscous sublayer the slope is 1, as in $\nu^{(t)}/\nu = B_1^+ y^+$. These need to be added in the right way to get the total viscosity, choosing the smaller of the two for the eddy kinematic viscosity. The coefficients B^+ and B_1^+ should be related to each other. Outside the boundary layer, the dissipation theorem may tell how $\nu^{(t)}/\nu$ depends on distance from the wall. On the figure, only one value of B_1^+ is shown, but four values of B^+ are shown.

1932 data on pipe flow, where Nikuradse [1] may not have recognized that his measured friction factors are not in harmony with his measured eddy viscosities.

The viscous sublayer is so thin, and the turbulence has decayed to such an extent, that eddies of the turbulence behave independently of each other. This permits application of Fourier transforms to explain the profile of the eddy viscosity and also that of the eddy diffusivity very close to the wall.

These diverse aspects of turbulence are reviewed in this article.

DISSIPATION THEOREM

Newton postulated that in a moving fluid the stress should be related locally to the spatial derivative of the velocity; the coefficient is called the viscosity μ. Turbulent flow is more complex and is characterized by rapid and apparently random fluctuations of velocity and pressure. This should also be governed by local relationships among certain statistical averages of the fluid motion. The statistical quantities can include principally the eddy viscosity and the volumetric dissipation but could also include the stress in the fluid and the energy density of turbulent eddies. The Reynolds stress is a momentum flux density or stress, being the density multiplied by averages of two fluctuating components of the velocity.

The eddy kinematic viscosity $\nu^{(t)}$ is defined as the coefficient between the average stress and the spatial derivative of the average velocity, very similar to Newton's flux relationship for laminar flow.

$$-\tau = \overline{\tau}_{xy} = -\rho(\nu + \nu^{(t)})\frac{\partial \overline{v}_x}{\partial y}. \quad (1)$$

Since the stress and velocity derivative are both tensors, the eddy kinematic viscosity is really a tensor with 81 components, but in many simple geometries one is mostly concerned with a scalar form of this equation. Hence, with an extra minus sign, τ can become a positive quantity. The volumetric dissipation is the double-dot product of the stress and the velocity derivative. In turbulent flow, dissipation is approximately related to the stress and the total viscosity.

$$\mathcal{D}_V = -\tau : \nabla \mathbf{v} \approx \frac{\tau^2}{\rho(\nu + \nu^{(t)})}. \quad (2)$$

To have enough equations to match the number of unknowns, one needs to postulate how volumetric dissipation $\mathcal{D}_V$ varies with time and position in response to convection, diffusion, and decay. This is the makeup of the dissipation theorem:

$$\frac{\partial \mathcal{D}_V}{\partial t} + \overline{\mathbf{v}} \cdot \nabla \mathcal{D}_V = \nabla \cdot \left[(\nu + \nu^{(t)})\nabla \mathcal{D}_V\right] - \frac{k(\mathcal{D}_V)^n}{\xi^p (R^+)^q}. \quad (3)$$

In the early examples, the tensorial nature of the eddy kinematic viscosity is ignored. The terms on the left describe time variation and convection of dissipation. The first term on the right assumes that the total kinematic viscosity plays the role of the diffusion of dissipation. The last term is the (dimensional) decay of the dissipation describing how dissipation will decay if left to itself. The dissipation is assumed to decay with a rate constant k and the second power of the volumetric dissipation itself ($n = 2$), although a first-order term can be added when the decay is small.

Empirical evidence is needed to establish the form of the decay term. Study of turbulent pipe flow [1] has been important for describing the decay. The theory of homogeneous isotropic turbulence should also be useful. Hopefully some generality becomes apparent so that one can predict turbulent flow in a variety of geometries and situations. From pipe flow, factors related to the stress and the Reynolds number with exponents of p and q are useful.

Figure 1 is designed to help the reader understand how different factors affect the eddy and total viscosity. The kinematic viscosity is always present and is dominant close to a solid wall. The eddy viscosity decreases near a solid wall, linearly in a region where the turbulent flow is dominant but with a y^3 depen-

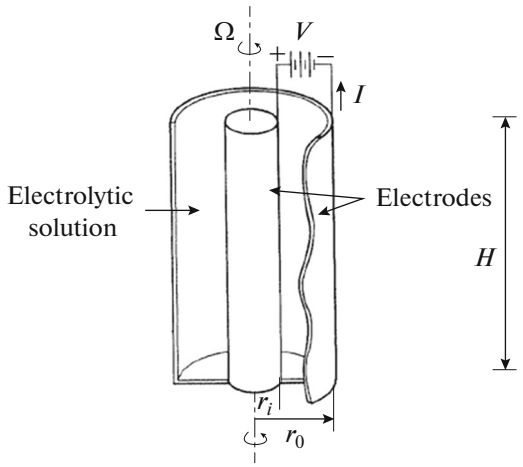

Fig. 2. Rotating cylinder system (from [8]).

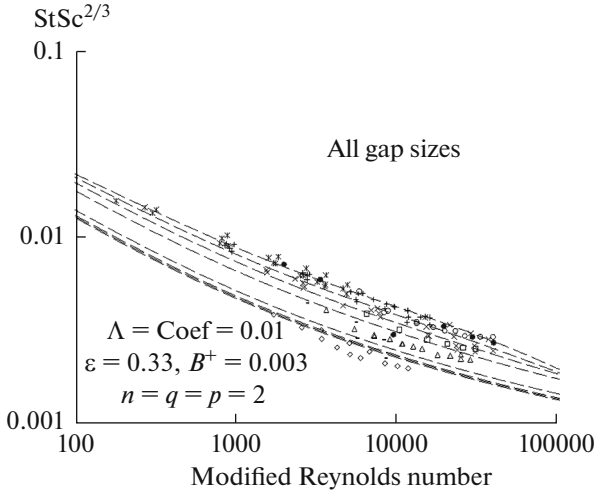

Fig. 3. Stanton number St versus modified Reynolds number for mass transfer to the inner rotating cylinder. The five sets of experimental data of Eisenberg have values of $1 - \kappa$ of 0.871, 0.7487, 0.633, 0.491, and 0.1723. The four sets of Mohr are for thinner gaps with $1 - \kappa$ of 0.0839, 0.0606, 0.0393, and 0.0172. The dashed lines are calculated with the dissipation theorem using the parameters on the figure. The symbols are the same as in Fig. 4.

dence in the viscous sublayer. This behavior is seen in many examples in this paper.

The first two examples, concentric cylinders and pipe flow, are geometries where the stress distribution can be predicted in advance. Consequently it is often convenient to use a stress parameter $R^+ = (R/\nu)(\tau_0/\rho)^{0.5}$ for the pipe and a similar R_i^+ based on the inner rotating cylinder radius. The next two examples are developing flows, one on a flat plate at zero incidence and one on a rotating disk. In both these systems, the flow is laminar near where it starts to flow by the solid, then has a transition to turbulence, and finally comes to a fully turbulent flow where the kinematic viscosity has a diminished role. There is an analogy here with the first two flows, which show progression as the stress parameter is increased. However, the lack of knowledge of the stress distribution requires that the momentum and continuity equations be solved simultaneously with the treatment of the dissipation equations.

ROTATING CYLINDERS

Fundamental studies of turbulent mass-transfer were made in an electrochemical system [6] where a rotating inner cylinder provides vigorous stirring and results in turbulent flow. This should be an ideal system for electrochemical studies because it is relatively compact, has a uniform current-density distribution, and can achieve high rates of mass transfer. It has been used in several studies of corrosion. It should also be valuable for studies of turbulence. Eisenberg does not make good use of the five different values of κ studied, but they are utilized in this work. Mohr [7] extends Eisenberg's values of κ to much thinner gaps. The stress distribution in the radial direction is easily calculated, although no measurements were reported on the overall stress or torque. The fact that the torque is easily measured and is directly related to the overall dissipation in the flow is also a motivating factor for studying this system in turbulent flow and for choosing the volumetric dissipation as a useful statistical quantity. The geometry of the system is shown in Fig. 2.

Figure 3 shows the data [6, 7] as the Stanton number St multiplied by the 2/3rds power of the Schmidt number. Eisenberg [6] uses a Reynolds number based on the radius of the inner cylinder

$$\mathrm{Re}_i = \frac{r_i^2 \Omega}{\nu}, \tag{4}$$

but a Reynolds number based on the gap distance would be more appropriate for thin-gap cells

$$\mathrm{Re}_g = \frac{r_i \Omega (r_0 - r_i)}{\nu}. \tag{5}$$

Consequently we prefer to use a modified Reynolds number

$$\mathrm{Re}_m = (1 - \kappa)\,\mathrm{Re}_i = \kappa\,\mathrm{Re}_g, \tag{6}$$

which spans the whole range of gaps.

The same data are shown in Fig. 4, where one can see more clearly how much the data deviate from the theory.

The data are fit well by the empirical formula

$$\mathrm{StSc}^{2/3} = A\,\mathrm{Re}_m^n\,\mathrm{Sc}^p. \tag{7}$$

The quality of the fit ranges from 0.03 to 0.13 for the different values of κ. The exponent n ranges from -0.46 to -0.28 with no strong pattern; A reflects this variation in n. However, the exponent p for the

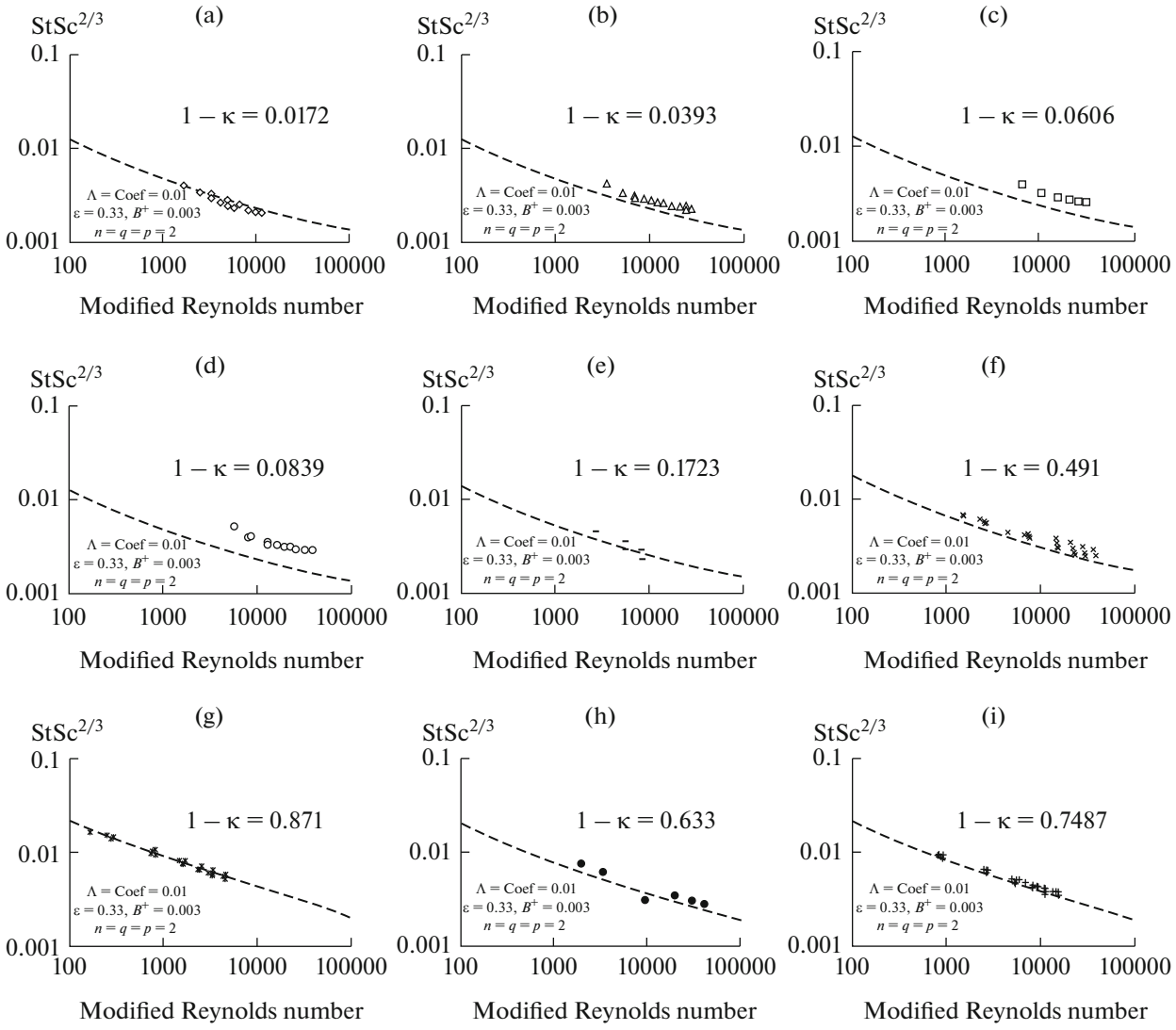

Fig. 4. Data for mass transfer to an inner rotating cylinder for various ratios κ of inner cylinder to outer cylinder radius. The predictions of dissipation theory drop gradually as the gap is decreased. The thin-gap data of Mohr are not harmonious with the thick-gap data.

Schmidt number is very close to –0.01, and therefore very close to the theoretical value for laminar mass transfer with high Sc. This exponent is also very close to the theoretical value for turbulent mass transfer if the eddy viscosity is proportional to y^3 in the viscous sublayer. (See also the section on the viscous sublayer). In contrast, Eisenberg ignores the different values of κ for which he took careful data and represented the fit of all his data by

$$\mathrm{StSc}^{2/3} = 0.0642\,\mathrm{Re}_i^{-0.3}\,\mathrm{Sc}^{0.0227}. \quad (8)$$

Thus, the sign of the exponent on Sc is opposite those fit to each value of κ. No single value of κ shows an exponent near 0.0227; they are closer to –0.01.

The dissipation theorem gives the dashed lines on Figs. 3 and 4 [8, 9]. One set of parameters is used for all values of κ. Predicted profiles of eddy viscosity and of volumetric dissipation are given in Figs. 5 and 6 for $1 - \kappa = 0.491$. Here $\xi = r/r_i$, and dissipation is made dimensionless with the value at the inner cylinder:

$$D = \frac{\mu \mathscr{D}_V}{\tau_i^2}, \quad (9)$$

where τ_i is the stress on the inner cylinder. D is multiplied by ξ^4 so that the value plotted is also 1 on the outer cylinder.

The eddy viscosity needs to go to zero on both solid surfaces, and it rises to a maximum in the middle of the fluid. From [1] we learn that the profiles should

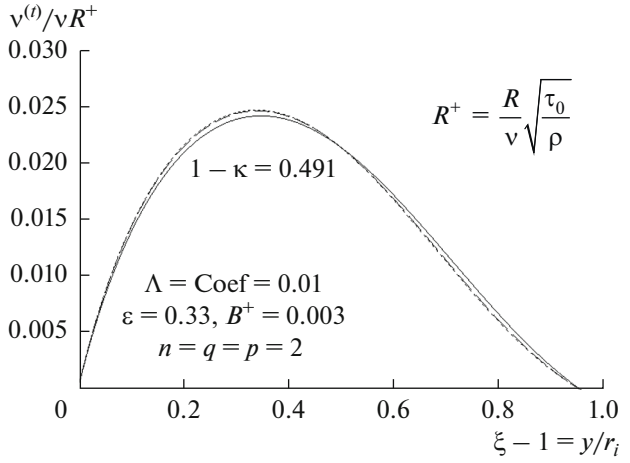

Fig. 5. Profiles of $\nu^{(t)}/\nu R_i^+$ against $\xi - 1$ for several values of R_i^+, and for $1 - \kappa = 0.491$. The upper curve with short dashes has $R_i^+ = 16399$, the curve with longer dashes has $R_i^+ = 3049$, and the solid curve has $R_i^+ = 567$.

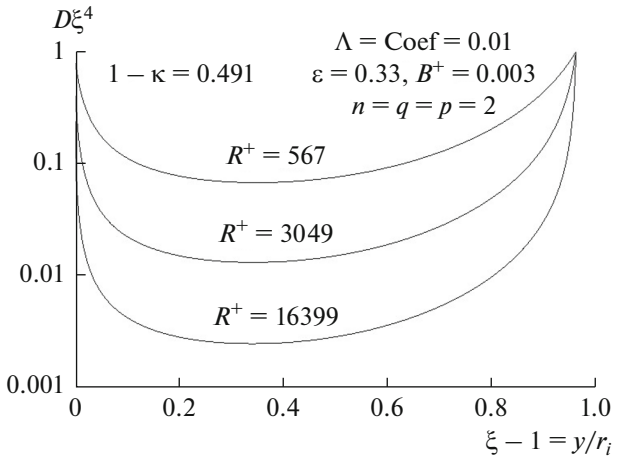

Fig. 6. Values of D multiplied by ξ^4, to bring them back to unity at the outer cylinder.

collapse onto a limit curve for large values of R_i^+. This is accomplished by having R_i^+ in the denominator of the decay term.

As plotted in Fig. 6 with a logarithmic scale on the ordinate, it becomes clear that the profiles of dissipation have the same shape in the central region, but they are constrained to come to the boundary condition on the two solid walls. The decay causes the dissipation to decrease away from the walls. Otherwise, the total friction (or torque) would be quite large.

Correct trends are given by the dissipation theorem. It provides a means to calculate the profiles of the dissipation and the eddy viscosity in regions away from the walls. This is shown well by Fig. 7, which shows an empirical factor with a single exponent on the Reynolds number, but now cross-plotted against the dimensionless gap distance, $1 - \kappa$. The individual values of $1 - \kappa$ are seen; the points for a given value of $1 - \kappa$ are spread because we did not use the best exponent n for each value of $1 - \kappa$ (and because of the inherent scatter of the data). Still some discrepant data points show up, like one for $1 - \kappa = 0.633$.

PIPE FLOW

The second example is steady, fully developed flow in a pipe. Fortunately, Nikuradse [1] in 1932 published extensive and very careful data over a wide range of Reynolds numbers. He was trying to explore very high Reynolds numbers because then available data never straightened out when friction factor against Reynolds number was plotted on a log–log scale. Nikuradse discovered an asymptotic region that showed a clear limiting behavior and led to the statement that no one ever needed to go to higher Reynolds numbers experimentally because the limiting behavior was clear. He measures accurate velocity and eddy viscosity profiles as well as overall friction factors for the flow. It was already known that, if one plotted the reciprocal of the square root of the friction on a linear scale against the Reynolds number times the square root of the friction factor on a logarithmic scale, one got a straight line. The data show clearly that the eddy viscosity goes through a maximum about halfway between the wall and the axis of the pipe. Then it declines toward zero, but it does not reach zero. Figure 8 shows his data for four intermediate Reynolds numbers. This provides an invaluable guide to the nature of turbulent flow, and it guides the development of the dissipation theorem. See [10, 11].

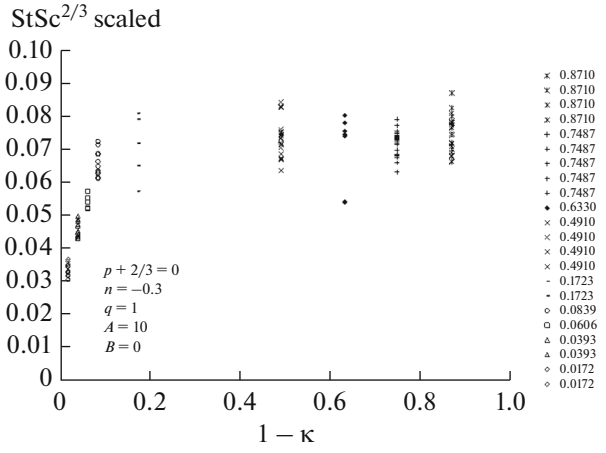

Fig. 7. The data of Eisenberg and of Mohr, plotted against gap distance. All data are plotted, including the discrepant point for $1 - \kappa = 0.633$.

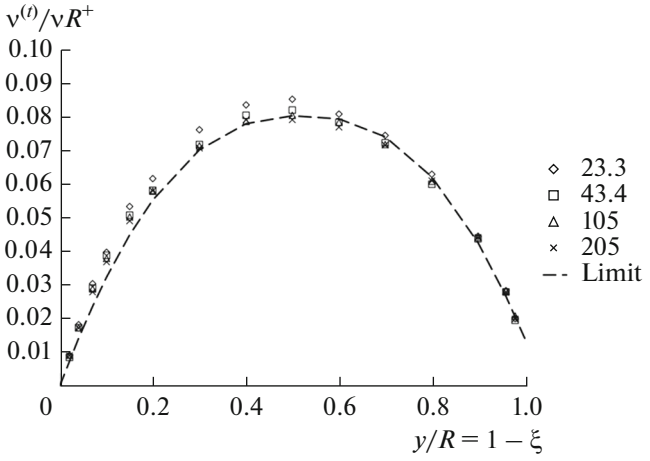

Fig. 8. Experimental profile of eddy viscosity, from [1]. Nikuradse studies 16 Reynolds numbers in pipe flow ranging from 4000 to 3.2 million. This graph shows four intermediate Reynolds numbers and a limit curve approached for very high Reynolds numbers. The values [1, 11] for lower Reynolds numbers lie progressively higher than the limit curve. Values of $\nu^{(t)}/\nu$ need to be divided by R^+ to cause the profiles to collapse onto the limit curve.

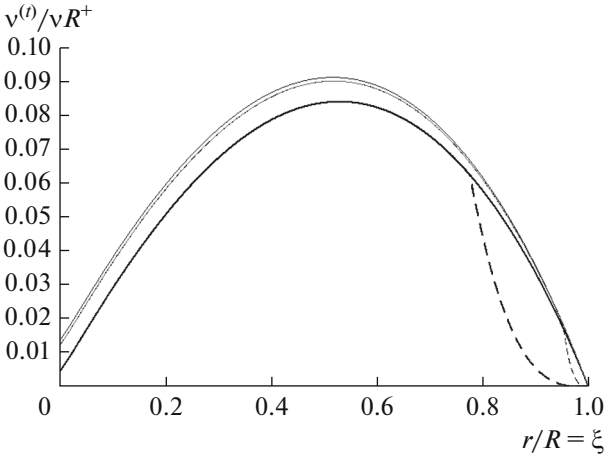

Fig. 9. Profiles of the eddy viscosity calculated with the dissipation theorem. The curves are calculated with the parameters Coef = $\Lambda = 0.17$, $n = p = q = 2$, $B^+ = 0.0005$, and $\varepsilon = 0.33$. Curves for R^+ of 88198, 16399, 3049, and 567 superpose, while that for 105 falls a little lower. (In contrast, Nikuradse's experimental data for low R^+ fall above his limit curve in Fig. 8). The solid curves are calculated by the dissipation theorem without regard for any y^3 region. Dashed curves for $R^+ = 567$ and 105 show the effect of splicing in the y^3 region. For $R^+ = 105$, this extends out from $r/R = 1$ to about 0.8, but much less far for $R^+ = 567$. (Compare Fig. 1). At the left, the curves mimic the curves of Nikuradse in Fig. 8 by not going to zero on the axis. This is accomplished by the ε parameter, introduced here.

To obtain concordance with experimental results, the decay term is expressed as

$$\text{decay} = \frac{\rho R^2}{\tau_0^2}\text{Decay} = \Lambda\left(\frac{DR^+}{\xi}\right)^2 + \Lambda\varepsilon\frac{D}{R^+}, \quad (10)$$

where Decay is the dimensional decay in equation (3), decay is a dimensionless decay, $\Lambda = 0.17$, and $\varepsilon = 0.33$. It is clear [11] that the decay term is mainly proportional to D^2 by reverse engineering of Nikuradse's eddy viscosity in Fig. 8. This produces by the dissipation theorem a profile that goes to zero on the center line. Addition of a term linear in D reproduces the profile of Fig. 8 that does not quite go to zero on the center line.

A few profiles of the eddy viscosity calculated from the dissipation theorem are shown in Fig. 9. Pipe flow differs from that in the rotating cylinder system not because one is rotating but because the shear stress goes to zero in the center of the pipe, whereas the shear stress is never zero in the cylinder system and stays constant for thin gaps.

Dimensionless dissipation calculated from Nikuradse's profiles of eddy viscosity (see Fig. 8) is shown in Fig. 10. The dashed line is the result for laminar flow in the pipe. The decay greatly reduces the dissipation so that it remains very high only near the wall. The decay term is adjusted (based on Nikuradse's measured eddy viscosity profiles), resulting in the form in equation (10). The short dashed curves on Fig. 10 show how the calculated dissipation can approach that for laminar flow (and consequent zero eddy viscosity) if ε is set to zero, with no adjusting the value of Λ.

Getting predictions of negative eddy viscosity was a persistent problem. It helped to understand that negative values arise when a calculated dissipation curve crosses the line for laminar flow, and Nikuradse's measured profiles of eddy viscosity eventually helped resolve the issue.

Originally we expected the eddy viscosity to be a maximum on the center line, but Nikuradse's experimental results (Fig. 8) show that the eddy viscosity actually goes through a maximum and approaches a small but nonzero value on the axis. The decay increases when the dissipation is large near the wall, and it increases even faster closer to the axis (due to the ξ^2 in the denominator of equation (10)). The shape of the dissipation curves in Fig. 10 reflects the decrease of D toward the axis but also the increase in the decay due to the radial position. When D becomes very small, the decay becomes small, and the curve can cross the laminar line.

The friction factor in pipe flow can be calculated from the equation [11]

$$\sqrt{\frac{2}{f}} = R^+\int_0^1 \frac{\xi^3 d\xi}{1 + R^+ M(\xi)}, \quad (11)$$

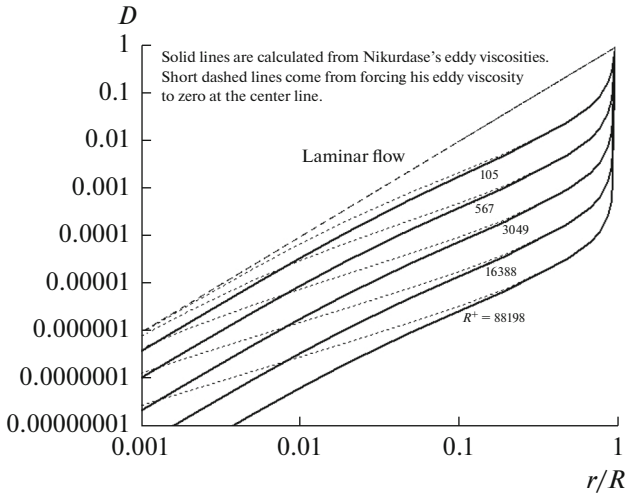

Fig. 10. Dimensionless dissipation for a range of values of the stress parameter R^+, calculated from set curves for the eddy viscosity. All the curves start at 1 at the wall ($r/R = 1$). Higher values of R^+ cause a steeper drop in the volumetric dissipation and thereby stay farther from the region of negative eddy viscosity. Solid curves follow Nikuradse's limit curve in Fig. 8. Short dashed curves come from forcing his limit curve to zero eddy viscosity on the center line and approach asymptotically the laminar line near the axis. This means that the dissipation program, which predicts the eddy viscosity, has a greater likelihood of touching the laminar line. The dissipation curves have the same shape on this scale, except near the wall, where the boundary condition states that $D = \mu\mathcal{D}_V \big/ \tau_0^2 = 1$.

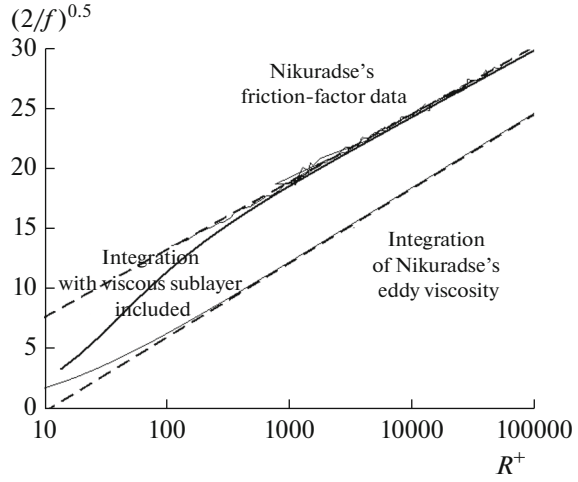

Fig. 11. Calculations of the friction factor from the distribution of eddy viscosity, plotted according to the universal-resistance law, which is supposed to yield a straight line. The curve toward the bottom is obtained by direct integration of equation (11) with the eddy viscosity measured by Nikuradse, with smaller step sizes for larger values of R^+. The other curve was calculated with the dissipation program, in essence using the profiles of eddy viscosity in Fig. 9 but with inclusion of the y^3 region. This curve rises from the lower curve and eventually approaches a straight line which is much higher than the asymptote with the lower curve. (Here $\Lambda = 0.17$, $n = p = q = 2$, $B^+ = 0.0005$. The curve is not modified when ε is nonzero and treated as in Fig. 9). The straight lines are $(2/f)^{0.5} = 2.7\ln(R^+) - 6.46$ for the lower line and $2.45\ln(R^+) + 2$ for the upper line, which agrees well with Nikuradse's fit of experimental friction-factor data, which extend from $R^+ = 112$ to 56000. His line matches the data shown but extends beyond it.

where $\xi = r/R$ and $M = \nu^{(t)}/\nu R^+$. Nikuradse [1] gives us measured friction factors over a wide range of Re or R^+. These are shown in Fig. 11. A surprising result [11] is that those friction factors do not agree with those calculated from equation (11) with Nikuradse's own measured profiles of the eddy viscosity, published in the same paper with the friction factors. My guess is that Nikuradse noticed this discrepancy but had no explanation. The first clear statement of the existence of the viscous sublayer came only later [3–5].

FLOW PAST A FLAT PLATE

The next two examples involve developing flow, where first there is laminar flow, followed by transition to turbulence and then fully developed turbulence. These are first for flow of a uniform stream past a flat plate at zero incidence and second for flow on a rotating disk. Figure 12 is a sketch of the system for the flat plate. In these two examples, the stress distribution is not known in advance, as it was for the rotating cylinder and pipe flow. Therefore one needs to include in the treatment the continuity equation and at least one tangential component of the momentum equation, in addition to the stress equation, the relationship of the dissipation to the eddy viscosity, and the dissipation theorem. The eddy diffusivity is also needed, unless it is taken to be equal to the eddy kinematic viscosity.

The Blasius solution describes the laminar boundary layer where the thickness of the region increases with the square root of the distance x along the plate and the wall stress τ_0 decreases with the reciprocal of the square root. We find it expedient to phrase the problem in terms of the coordinate system used by Blasius. Thus, for normal and tangential dimensionless distance variables, we use

$$\eta = y\sqrt{\frac{V_\infty}{\nu x}} \quad \text{and} \quad \chi = \frac{xV_\infty}{\nu} = \mathrm{Re}_x, \tag{12}$$

and for dimensionless tangential and normal velocity components we use

$$\bar{V}_x = V_\infty \frac{\partial f(\chi,\eta)}{\partial \eta} \quad \text{and}$$
$$\bar{V}_y = \sqrt{\frac{\nu V_\infty}{x}}\left[\frac{\eta}{2}\frac{\partial f}{\partial \eta} - \frac{f}{2} - \chi\frac{\partial f}{\partial \chi}\right], \tag{13}$$

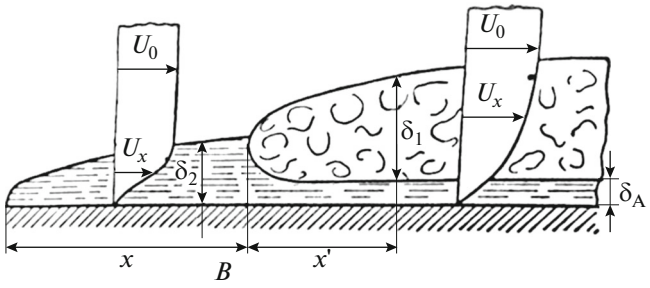

Fig. 12. Schematic picture of different regions of flow on a flat plate in a uniform stream (taken from [12]). Near the leading edge, there is laminar flow. x' denotes a region of transition to turbulence, and to the right there is to be a region of fully developed turbulence, which we should like to characterize. There is also a small elliptic region very close to the leading edge. At a given distance downstream in the turbulent region, there is a thin viscous sublayer next to the plate where the eddy kinematic viscosity is nonzero but smaller than the kinematic viscosity. Outside this there is a region where the kinematic viscosity is smaller than the eddy kinematic viscosity. Still farther out there is a region where some turbulence remains, but the tangential average velocity has reached its value in the external flow. (The figure should show U_0 to be the same magnitude at both positions on the plate.) The region of significant eddy kinematic viscosity may extend a great distance from the plate, but it may have little effect on the average flow because the stress and the gradient of the average velocity are small.

which already satisfy the continuity equation. Dimensionless stress, volumetric dissipation, and total viscosity are introduced as follows

$$T = \frac{\tau}{\mu}\sqrt{\frac{\nu x}{v_\infty^3}}, \quad D = \frac{x\mathcal{D}_V}{\rho v_\infty^3}, \quad \text{and} \quad G = \frac{\nu + \nu^{(t)}}{\nu}. \quad (14)$$

Here D is defined differently from the dimensionless volumetric dissipation used in the first two examples. We use the total viscosity since it makes the equations simpler, so that $G = 1$ for laminar flow and also on the surface of the solid plate.

The governing differential equations, after the coordinate transformation from x, y to χ, η, are the momentum equation (combined with the continuity equation)

$$2f'\chi\frac{\partial f'}{\partial \chi} - 2f''\chi\frac{\partial f}{\partial \chi} = ff'' + 2\frac{\partial Gf''}{\partial \eta}, \quad (15)$$

the dissipation theorem

$$2f'\chi\frac{\partial D}{\partial \chi} - 2\frac{\partial D}{\partial \eta}\chi\frac{\partial f}{\partial \chi} = 2Df' + f\frac{\partial D}{\partial \eta} + 2\frac{\partial}{\partial \eta}\left(G\frac{\partial D}{\partial \eta}\right) - 2\Lambda\frac{\chi^{2-n}D^n}{\xi^p(R^+)^q}, \quad (16)$$

the stress relation

$$T = Gf'', \quad (17)$$

and the equation relating volumetric dissipation and stress

$$GD = T^2, \quad (18)$$

where we adopt the definitions

$$f' = \left(\frac{\partial f}{\partial \eta}\right)_\chi \quad \text{and} \quad f'' = \left(\frac{\partial f'}{\partial \eta}\right)_\chi. \quad (19)$$

It should be understood that χ is held constant for any derivative with respect to η, and vice versa. After the coordinate transformation is complete, there are only these two independent variables.

For laminar flow equation 15 reduces to the equation of Blasius, where f does not depend on x and where $\nu^{(t)} = 0$. Thus, we can solve this equation starting at $x = 0$. After the eddy viscosity builds up, the solution will deviate from the Blasius solution. The other equations are needed to treat this buildup of the eddy viscosity.

The meaning of the factors in the decay term in equation (16) remains in question. One replaces ξ with the stress T, in harmony with pipe flow. Three replacement candidates for R^+ occur. One is χ, and another is $x^+ = (x/\nu)(\tau_0/\rho)^{0.5}$. Both introduce an x dependence into the decay term. A third possibility is $(\tau_0/\rho)^{0.5}/\nu_\infty$, which retains the stress at the wall but avoids the distance x. We pursue this last one. We may also introduce an εD term as in equation (10), but this may introduce an undesired dependence on x into the decay term.

The problem proves to be very difficult to solve numerically. For fully developed turbulence, a back-substitution method proved useful. The profile of G is taken to be known, starting with an assumption that $G = 1$. The other equations are much more stable if G is specified. This means that equation (18) is not used in this process, but after profiles for f, f', T, and D are obtained, a new guess for the G profile is obtained from equation (18) and the now known profiles of T and D. After several iterations, the calculated profile for G agrees with that assumed, and convergence is achieved.

Report on the development of the flow with distance x must wait for the future.

For laminar flow, $G = 1$, and equation 18 shows that D should equal T^2. However, the value calculated for D from the dissipation theorem does not equal T^2. This discrepancy provides a driving force for the creation of turbulence. It also means that whenever $D = T^2$, the eddy viscosity is zero, similar to the behavior with pipe flow (see Fig. 10).

One of the problems is that the curve for D can cross that for T^2. This means that the eddy viscosity has dropped to zero. Since this is aphysical, G is set to 1. Then there is a sharp dividing line between a region with eddy viscosity and a region with none.

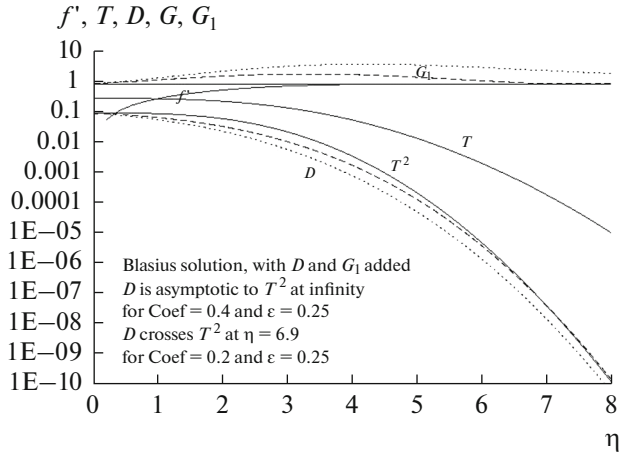

Fig. 13. Blasius solution for laminar flow, with $G = 1$. The values for T and f' then do not depend on the decay parameters. D values do not agree with T^2, which they should for laminar flow on a flat plate. For the decay parameters for the long dashed lines, D crosses T^2, and therefore the estimated G_1 profile goes to 1 at a finite value of η. For the decay parameters with the short dashes, the lines do not cross, and therefore the estimated G_1 extends much farther, perhaps even to infinity.

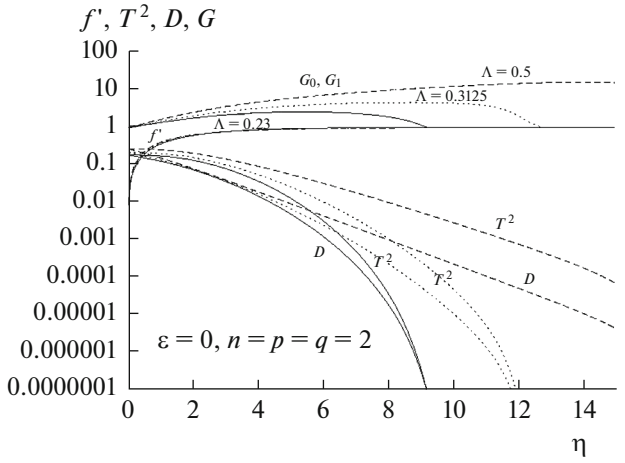

Fig. 14. Converged solutions for fully developed turbulent flow on a flat plate. This means that the graph stays the same as x increases, but the thickness of the boundary layer continues to increase with the square root of distance along the plate. Compare Fig. 12.

When we focus on fully developed flow, we solve the above equations without the derivatives with respect to χ. Thus the independent variable is only η, and the only parameters arise from the decay.

Figure 13 illustrates laminar Blasius flow (with $G = 1$) but also shows the possibility of the calculated D crossing the T^2 curve, which implies negative values of the eddy viscosity.

Figure 14 shows three converged solutions for fully developed turbulent flow on a flat plate, with Λ = 0.23, 0.3125, and 0.5, all with ε = 0. For each set, $G_0 = G_1$. The turbulence can extend farther out by adjusting Λ. The profile for f' does not change much; it extends out a little farther than the Blasius solution in Fig. 13, and it has a higher value of T at the wall. Since the dimensionless tangential velocity is 1 at infinity, there is little that the profile can change. D and T^2 extend substantially farther out than in Fig. 13, and they become straighter, thus showing an exponential decrease with distance.

It should be pointed out that the value of T at η = 0 does not represent the stress actually on the plate. Put another way, the viscous sublayer introduces an apparent slip velocity at the surface, where the dissipation theorem does not consider the y^3 behavior in the viscous sublayer. Figure 11 shows that there is substantial stress in the viscous sublayer, and this needs to be accounted for to get the actual friction factor.

Next one wants to follow the developing turbulent boundary layer. This will have to wait. It takes a long time to calculate out to large values of χ. Also, preliminary results suggest that the turbulence comes in sooner than experiments would suggest, and the frictional aspect of the viscous sublayer is not implemented yet. It is easy for the computer program to develop a profile that is not sustainable. One might think that a profile where D crosses T^2 is not proper. However, if D does not cross but instead drops well below the curve for T^2, equation 18 yields huge values for the eddy viscosity, as contained in G. Figure 15 shows a profile that represents expected behavior of

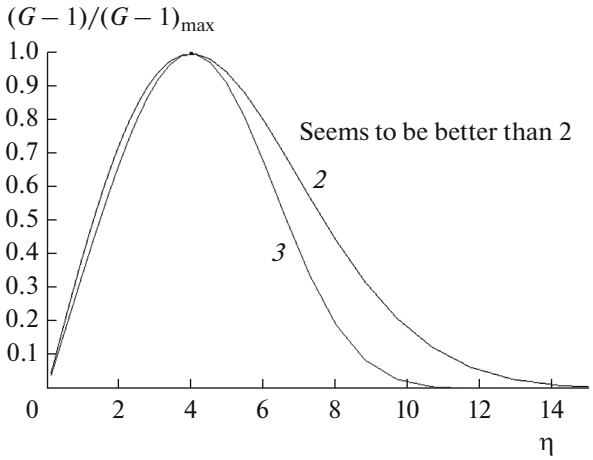

Fig. 15. Expected behavior for the eddy viscosity $G - 1$ on a flat plate. A form which looks like some calculated profiles can be expressed as

$$\frac{G-1}{(G-1)_{\max}} = \frac{\eta}{H\exp(-1/s)}\exp[-(\eta/sH)^s], \qquad (20)$$

where H is the value of η at the maximum and s is a constant. $s = 3$ reproduces the desired shape better than $s = 2$.

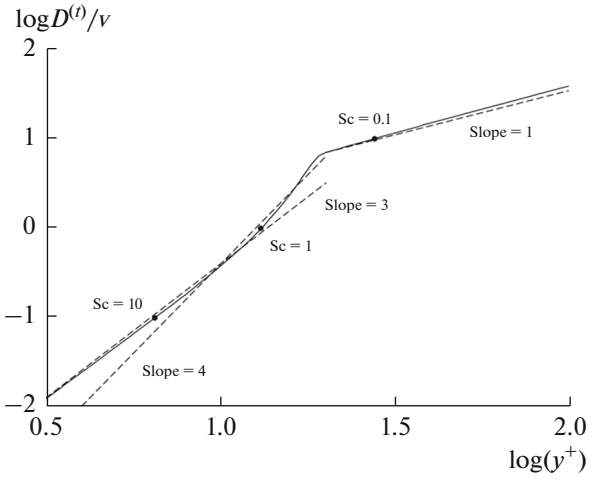

Fig. 16. Profile of the eddy diffusivity in the region near the wall in turbulent shear flow [16, 17]. Dashed lines with slopes of 1, 3, and 4 are superposed on the profile, suggesting that $\mathcal{D}^{(t)}/\nu$ is proportional to y^3 very close to the wall, proportional to y^4 just inside the viscous sublayer, and proportional to y in the outer turbulent flow just outside the viscous sublayer. Solid dots are also added to indicate the thickness of the diffusion layer for different values of the Schmdt number. This thickness is defined as the distance at which $\mathcal{D}^{(t)} = \mathcal{D}$. The dot for Sc = 100 is just to the left of the range of the graph, and that for Sc = 1000 is substantially to the left of this range.

$G - 1$ as a function of η; it should rise to a maximum value and then decline gradually to zero. It should not begin to rise again after the maximum.

FLOW TO A ROTATING DISK

The fourth example is a rotating disk, a favorite tool for electrochemical systems. References [13–15] cover some old turbulence work with this system. Experimentally it is probably much more convenient than a large flat plate in a wind tunnel because it is more compact and easier to keep clean. The analysis should proceed much like that for the flat plate, and it may be equally difficult.

HOMOGENEOUS ISOTROPIC TURBULENCE

In 1941 Kolmogorov [2] published a theoretical prediction of how homogeneous isotropic turbulence would decay. He states that large eddies are not acted on by viscosity. They grind against each other and create smaller eddies. However, the kinetic energy in these eddies remains the same. This process continues until the eddies become so small that viscosity does degrade the kinetic energy into thermal energy. This process should be closely related to the decay of dissipation discussed here.

VISCOUS SUBLAYER

There is great interest in what goes on very close to a solid surface in turbulent shear flow. It was proposed in 1932 and again in 1942 that this region is not laminar but that instead the eddy viscosity decreases gradually as the distance from the surface decreases. There has been disagreement as to whether the eddy diffusivity is proportional to the third power or the fourth power of distance from the surface. The truth is that it is proportional to the cube very close to the surface but to the fourth power near the outer limit of the viscous sublayer. One can see this in Fig. 16 [16, 17].

In comparison with Fig. 1, one can recognize that the horizontal line for ν on Fig. 1 becomes a horizontal line for $\mathcal{D}$ in Fig. 16 at an ordinate value of 1/Sc. This provides a greater range of y over which to study the eddy diffusivity in the viscous sublayer, although this does not constitute a direct measurement of $\mathcal{D}^{(t)}$.

Hopefully Fig. 16 resolves the disagreement. In the literature, several references favor the y^4 result, but experimental results of mass-transfer rates at high Schmidt numbers generally favor the y^3 situation, including those with the rotating cylinder system in Fig. 3. We mention that the Stanton number is nearly proportional to the −2/3rd power of the Schmidt number, which follows from the y^3 dependence of the eddy diffusivity and not the y^4 dependence. The mass-transfer rate reflects an average of the eddy diffusivity over the thickness of the diffusion layer. Figure 17 shows calculated values of $\mathrm{StSc}^{2/3}$ plotted against Sc for pipe flow for various values of R^+. At high Sc, the slope of the curves approaches zero not only if they are calculated with a y^3 dependence in the diffusion layer but also if they are calculated with the profile of $\mathcal{D}^{(t)}/\nu$ shown in Fig. 16. Only the curve calculated with a y^4 dependence throughout the diffusion layer shows a slope of −1/12 at high Sc, indicating that it is the asymptotic forms of the curves that show up most clearly and that the detailed behavior in the middle is less important. (A line with a slope of −1/12 is shown for comparison.) The distinction between slopes that differ by only 1/12 is hard to discern experimentally, especially since the mass-transfer results are frequently plotted against the Reynolds number instead of the Schmidt number.

Substantial clarification of the eddy diffusivity and the eddy viscosity in the viscous sublayer can also come from a statistical treatment of fluctuations in this region [19–21]. The eddy viscosity follows a y^3 dependence through most of the viscous sublayer, but the eddy diffusivity shows more structure and a dependence on the Schmidt number. While the two quantities may be substantially the same in the external turbulent bulk (outside the viscous sublayer), $\mathcal{D}^{(t)}$ can become much smaller than $\nu^{(t)}$, and the more so the larger the Schmidt number.

Levich [12, section 4, p. 29] says, "In the viscous sublayer Re is less than unity, and the second-order terms in the Navier–Stokes equations are small compared to the first-order terms. The velocity distribution in a viscous sublayer can therefore be determined by linear equations only. If a certain spectrum of eddies penetrates a viscous sublayer, the interaction between separate eddies ceases. The flow then becomes a sum of independent periodic motions, whose period T remains constant throughout the viscous sublayer."

Martem'yanov, Vorotyntsev, and Grafov [19] treat the sublayer and conclude that the eddy viscosity is proportional to y^3 but that the eddy diffusivity begins to deviate from the eddy kinematic viscosity within the viscous sublayer, showing a y^4 dependence just within the sublayer but having a y^3 dependence deep in the layer whose coefficient depends on the diffusion coefficient $\mathscr{D}$. They conclude that in the y^3 region the eddy diffusivity is proportional to the square root of $\mathscr{D}$. Martemianov [20] summaries statistical treatments of the viscous sublayer.

In analysis of turbulent flow, one writes all flow quantities as the sum of a steady part and a fluctuating part, for example,

$$\mathbf{v} = \overline{\mathbf{v}} + \mathbf{v}'. \tag{21}$$

One derives the equation for the fluctuations of the velocity by first averaging the momentum equation and then subtracting this result from the unaveraged equation. The result is

$$\frac{\partial \mathbf{v}'}{\partial t} + \nabla \cdot \overline{\mathbf{v}}\mathbf{v}' + \nabla \cdot \mathbf{v}'\overline{\mathbf{v}} + \nabla \cdot \mathbf{v}'\mathbf{v}' - \nabla \cdot \langle \mathbf{v}'\mathbf{v}' \rangle = \nu \nabla \cdot \nabla \mathbf{v}' - \frac{1}{\rho}\nabla \mathscr{P}', \tag{22}$$

$\mathscr{P}$ is the dynamic pressure. In the viscous sublayer, we drop terms quadratic in the fluctuations on the grounds that they are small compared with first-order terms. Rectangular coordinates are appropriate for the thin viscous sublayer. The continuity equation is treated the same way, but being linear it yields a simpler result. The equation of convective diffusion

$$\frac{\partial c_i}{\partial t} + \nabla \cdot (\mathbf{v} c_i) = \mathscr{D} \nabla \cdot \nabla c_i \tag{23}$$

is treated the same way. Since it has a nonlinear term, averaging generates a turbulent-transport term. With boundary conditions of

$$c_i = c_0 \quad \text{at} \quad y = 0 \quad \text{and} \quad c_i \to c_\infty \quad \text{as} \quad y \to \infty, \tag{24}$$

it is convenient to work with a dimensionless concentration defined as

$$\theta = \frac{c_i - c_0}{c_\infty - c_0}. \tag{25}$$

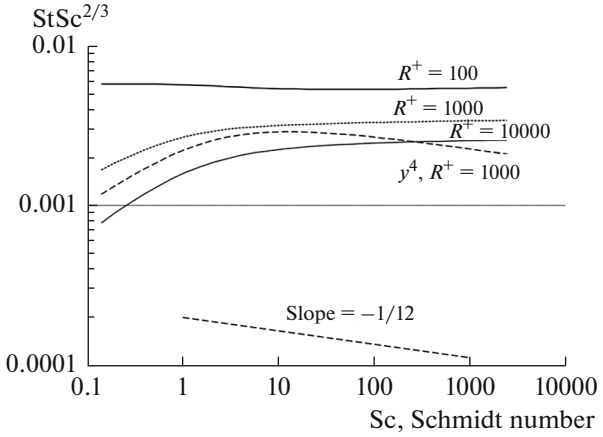

Fig. 17. Plot to show how the eddy diffusivity should affect the mass-transfer rate in pipe flow with a constant wall flux. The solid lines show how the Stanton number depends on the Schmidt number for three values of the stress parameter R^+ of 100, 1000, and 10000 (corresponding to Reynolds numbers of 2245, 36105, and 378600). For these curves, the eddy diffusivity is proportional to y^3 in the viscous sublayer. The curve with long dashes has a y^4 dependence in the viscous sublayer and has a slope of $-1/12$ for large Schmidt numbers. The curve with short dashes uses the dependence for the eddy diffusivity given in [18, equation (15.71)]. It essentially coincides with the curve for the same value of R^+ but a simple proportionality to y^3 in the viscous sublayer. These curves have a zero slope at large Sc and never show a slope of $-1/12$.

The complete set of equations for the fluctuations of velocity, pressure, and concentration is

$$\frac{\partial v_x'}{\partial x} + \frac{\partial v_y'}{\partial y} + \frac{\partial v_z'}{\partial z} = 0. \tag{26}$$

$$\frac{\partial v_x'}{\partial t} + \beta y \frac{\partial v_x'}{\partial x} + \beta v_y' = \nu \left(\frac{\partial^2 v_x'}{\partial x^2} + \frac{\partial^2 v_x'}{\partial y^2} + \frac{\partial^2 v_x'}{\partial z^2} \right) - \frac{1}{\rho}\frac{\partial \mathscr{P}'}{\partial x}. \tag{27}$$

$$\frac{\partial v_y'}{\partial t} + \beta y \frac{\partial v_y'}{\partial x} = \nu \left(\frac{\partial^2 v_y'}{\partial x^2} + \frac{\partial^2 v_y'}{\partial y^2} + \frac{\partial^2 v_y'}{\partial z^2} \right) - \frac{1}{\rho}\frac{\partial \mathscr{P}'}{\partial y}. \tag{28}$$

$$\frac{\partial v_z'}{\partial t} + \beta y \frac{\partial v_z'}{\partial x} = \nu \left(\frac{\partial^2 v_z'}{\partial x^2} + \frac{\partial^2 v_z'}{\partial y^2} + \frac{\partial^2 v_z'}{\partial z^2} \right) - \frac{1}{\rho}\frac{\partial \mathscr{P}'}{\partial z}. \tag{29}$$

$$\frac{\partial \theta'}{\partial t} + \beta y \frac{\partial \theta'}{\partial x} + v_y' \frac{\partial \overline{\theta}}{\partial y} = \mathscr{D} \left(\frac{\partial^2 \theta'}{\partial x^2} + \frac{\partial^2 \theta'}{\partial y^2} + \frac{\partial^2 \theta'}{\partial z^2} \right). \tag{30}$$

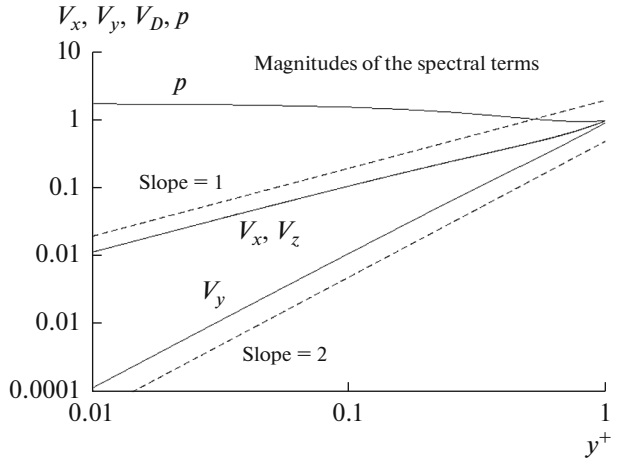

Fig. 18. Calculated profiles of the fluctuating components of the velocity and of the pressure for one component of the Fourier spectrum (for $K_x = K_z = \Omega = 1$). Here, B is taken to be 1. V_x, V_y, and V_z are taken to be zero at the wall. V_x and V_z and p are taken to be 1 at $y^+ = 1$. While the fluctuations are comparable in the three coordinate directions in the outer turbulent flow, the normal component decreases with a slope of 2 (in the log–log plot) in the inner part of the viscous sublayer, while the tangential components are nearly equal to each other and adopt a slope of 1. The pressure fluctuations persist with little change all the way to the surface.

Equqtion (30) is essentially identical to equation (6) in [21]. This constitutes a linear problem for the variation of the fluctuations if we know the average quantities. Due to the thinness of the viscous sublayer we have approximated the average velocity profiles as $\overline{v}_x = \beta y$, where β is a constant, and $\overline{v}_y = \overline{v}_z = 0$. The average concentration also depends only on y. We see from the third term in equation 30 that the concentration fluctuations arise due to interaction of the velocity fluctuations with the gradient of the average concentration. Concentration fluctuations are negligible outside the diffusion layer, which is very thin at high Sc (see Fig. 16).

Since the problem is linear and has sinusoidal variations in time and in the x and z directions, we can use Fourier transforms to separate the behavior of the various spectral components.

$$v_x' = \mathrm{Re}\{V_x(y)\exp(ik_x x + ik_z z + i\omega t)\}. \quad (31)$$

$$v_y' = \mathrm{Re}\{V_y(y)\exp(ik_x x + ik_z z + i\omega t)\}. \quad (32)$$

$$v_z' = \mathrm{Re}\{V_z(y)\exp(ik_x x + ik_z z + i\omega t)\}. \quad (33)$$

$$\mathcal{P}' = \mathrm{Re}\{P(y)\exp(ik_x x + ik_z z + i\omega t)\}. \quad (34)$$

$$\theta' = \mathrm{Re}\{C(y)\exp(ik_x x + ik_z z + i\omega t)\}. \quad (35)$$

Next make the problem dimensionless by introducing $y^+ = (y/\nu)(\tau_0/\rho)^{0.5}$ and dimensionless Fourier coefficients and a dimensionless pressure. The velocity functions V_x, V_y, and V_z, can be understood to be divided by the value of V_x at $y = \delta_0$. The parameters and dependent variables are defined according to:

$$K_x = k_x \frac{\nu}{v^*}, \quad K_z = k_z \frac{\nu}{v^*}, \quad \text{where} \quad v^* = \sqrt{\frac{\tau_0}{\rho}}. \quad (36)$$

$$\Omega = \omega \frac{\nu}{(v^*)^2}, \quad B = \beta \frac{\nu}{(v^*)^2}, \quad \text{and} \quad p = \frac{P}{\rho v^*}. \quad (37)$$

The parameters v*, ρ, and τ_0 are eliminated, and the problem is simplifies by having dimensionless Fourier variables K_x, K_z, and Ω. Substitution of equations (31) through (35) into equations (26) through (30) for each spectral component separately (each spectral component being the variables V_x, V_y, V_z, p, and C for a given set of K_x, K_z, and Ω) yields a set of ordinary differential equations:

$$iK_x V_x + \frac{dV_y}{dy^+} + iK_z V_z = 0. \quad (38)$$

$$i\Omega V_x + By^+ iK_x V_x + BV_y = -K_x^2 V_x + \frac{d^2 V_x}{dy^{+2}} - K_z^2 V_x - iK_x p. \quad (39)$$

$$i\Omega V_y + By^+ iK_x V_y = -K_x^2 V_y + \frac{d^2 V_y}{dy^{+2}} - K_z^2 V_y - \frac{dp}{dy^+}. \quad (40)$$

$$i\Omega V_z + By^+ iK_x V_z = -K_x^2 V_z + \frac{d^2 V_z}{dy^{+2}} - K_z^2 V_z - iK_z p. \quad (41)$$

$$i\omega C + \beta y i k_x C + V_y \frac{\partial \overline{\theta}}{\partial y} = \mathcal{D}\left(-k_x^2 C + \frac{d^2 C}{dy^2} - k_z^2 C\right). \quad (42)$$

Figure 18 shows the magnitudes of the spectral components for the velocity and the pressure for $K_x = K_z = \Omega = 1$. Magnitudes of the concentration fluctuations are shown in Fig. 19 for several values of the Schmidt number.

The Reynolds stress equals the density multiplied by the average of the product of the fluctuations of the y and x components of the velocity. Division by the density and the derivative of the average x component of the velocity gives the eddy kinematic viscosity. The turbulent mass-transport flux density is equal to the average of the product of the fluctuations of the concentration and the y component of the velocity. Division by the derivative of the average concentration gives the eddy diffusivity. These are shown in Fig. 20.

Figure 20 can be compared with the left side of Fig. 16, that is, with the viscous sublayer. The eddy

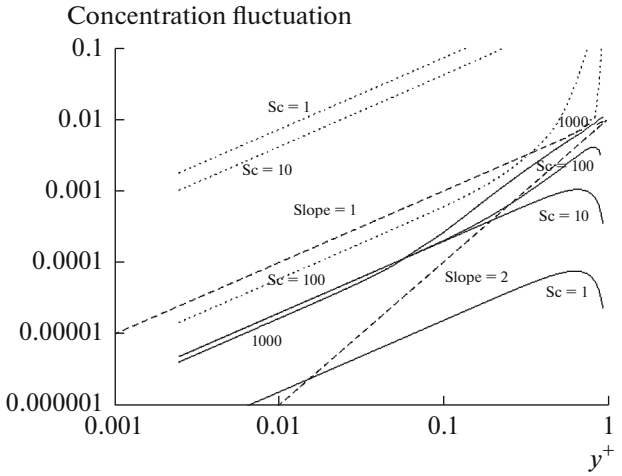

Fig. 19. Magnitudes of the fluctuations in concentration for four different Schmidt numbers Sc, ranging from 1 to 1000. Solid curves use a zero boundary condition for C at $y^+ = \delta_0^+ = 1$. Then the concentration fluctuations are due entirely to velocity fluctuations within the viscous sublayer. The curves with short dashes set C to 1 at $y^+ = \delta_0$, which might be more appropriate for Sc = 1 because the diffusion layer can extend somewhat beyond the viscous sublayer. For Sc = 1000, the two curves nearly coincide except for y^+ values very close to ${\delta_0}^+$. Dashed lines show for comparison slopes of 1 and 2.

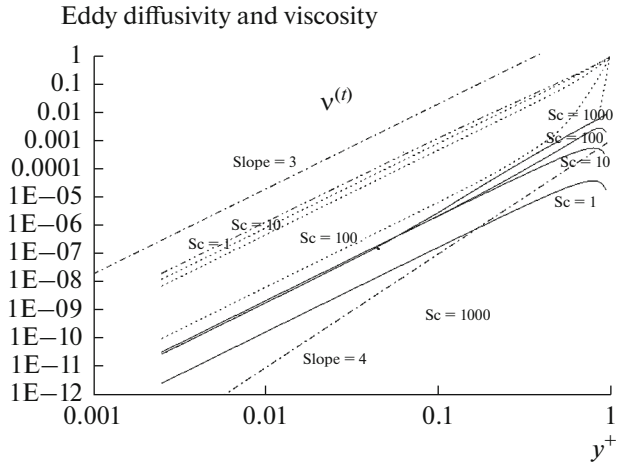

Fig. 20. Profiles of the relative magnitude of the eddy diffusivity $\mathscr{D}^{(t)}$ and the eddy kinematic viscosity $\nu^{(t)}$. The Schmidt number is a parameter for the diffusivities, and again, the boundary condition was taken as $C = 1$ for the short dashed lines and $C = 0$ for the solid lines, both boundary conditions applying at $y^+ = \delta_0^+ = 1$. The boundary conditions provide some distortion near the maximum value. The eddy kinematic viscosity is positioned just above the short dashed line for Sc = 1. Dot-dash lines provide comparison for slopes of 3 and 4.

kinematic viscosity shows nearly a y^3 dependence throughout the thickness of the viscous sublayer. The behavior of the eddy diffusivity depends a lot on the value of the Schmidt number. Toward the left, it is proportional to y^3, but for Sc = 100 and 1000 it shows a y^4 dependence just inside the viscous sublayer, say for y^+ between 0.1 and 1. Since the diffusion layer thickness lies at about 0.08 for Sc = 1000, the diffusion layer lies mostly in the y^3 region.

A long-standing goal is to relate the turbulence at some distance from the wall to that in the viscous sublayer, that is, to relate B_1^+ to B^+, where B_1^+ is the coefficient of the curve on the right side of Fig. 16 and B^+ is the coefficient of the y^3 term on the left side. We see from Fig. 20 that this ratio can depend on the Schmidt number and more particularly that the value of B^+ for Sc = 1000 could be lower by a factor of 1000 below that which would correspond to the slope of the y^3 term for the eddy kinematic viscosity. We can visualize a revision of the figure in [18], or in Fig. 16 here, to show curves for more than one Sc and also to show the curve for the eddy kinematic viscosity, which might lie on top of the curve for $\mathscr{D}^{(t)}/\nu$ for Sc = 1. A different value of B^+ is probably appropriate for friction-factor and torque data instead of mass-transfer data.

Neglect of interaction of eddies (that is, nonlinear effects) ceases to be valid at greater distances from the wall. It retains validity closer to the wall and therefore yields valid results for diffusion at high Schmidt numbers.

CONCLUSIONS

One seeks a unified theory of turbulent shear flow, whereby phenomena in different systems (like the four examples here) have similar causes, embodied in the dissipation theorem (augmented by the theory of the viscous sublayer). It seems, even at this stage, that different parameters might be required for different systems, but one hopes for unity eventually. One statement we can make is that rotating systems, like the cylinders and the disk, may not require a different theory if one takes into account the fact that the stress goes to zero at the axis of the pipe but does not in Couette flow or circular Couette flow. The dissipation theorem gives predictions for the dissipation and the eddy viscosity at distances away from the wall.

The foundation of the dissipation theorem is shaky, but it performs better than might be expected. One sees how important good experimental data are from the effect of Nikuradse's clarification of the behavior of turbulence in pipe flow. Even Kolmogorov theory should have a place here in clarifying the nature of the decay of turbulence.

COMPLIANCE WITH ETHICAL STANDARDS

The author declares that he has no conflict of interest.

REFERENCES

1. Nikuradse, J., Gesetzmässigkeiten der turbulenten Strömung in glatten Rohren, *Forschungsheft 356*, Beilage zu Forschung auf dem Gebiete des Ingenieurwesens, Edition B, Volume 3, September/October, 1932 (Berlin NW7: VDI-Verlag GMBH, 1932). Translated as Nikuradse, J. Laws of Turbulent Flow in Smooth Pipes, NASA TT F-10, 359 (Washington: National Aeronautics and Space Administration, October, 1966).
2. Kolmogorov, A.N., Dissipation of energy in locally isotropic turbulence, *Dokl. Akad. Nauk,* 1941, vol. 32, p. 16.
3. Murphree, E.V., Relation between heat transfer and fluid friction, *Ind. Eng. Chem.*, 1932, vol. 24, p. 726. https://doi.org/10.1021/ie50271a004
4. Levich, B., The theory of concentration polarization, I, *Acta Physicochim. URSS,* 1942, vol. 17, p. 257.
5. Levich, B., The theory of concentration polarization, II, *Acta Physicochim. URSS,* 1944, vol. 19, p. 117.
6. Eisenberg, M., Studies of rates of solid dissolution and of electrode reactions at rotating cylindrical bodies, *Dissertation,* Berkeley: Univ. of California, 1953.
7. Mohr, C.M., Jr., Mass transfer in rotating electrode systems, *Dissertation,* Berkeley: Univ. of California, 1975.
8. Newman, J., Theoretical analysis of turbulent mass transfer with rotating cylinders, *J. Electrochem. Soc.*, 2016, vol. 163, p. E191.
9. Newman, J., Turbulent flow with the inner cylinder rotating, *Russ. J. Electrochem.*, 2019, vol. 55, p. 44.
10. Newman, J., Application of the dissipation rheorem to rurbulent flow and mass transfer in a pipe, *Russ. J. Electrochem.*, 2017, vol. 53, p. 1061.
11. Newman, J., Further thoughts on turbulent flow in a pipe, *Russ. J. Elecrochem.*, 2019, vol. 55, p. 34. https://doi.org/10.1134/S1023193519010105
12. Levich, V.G., *Physicochemical Hydrodynamics*, Englewood Cliffs, NJ: Prentice-Hall, 1962.
13. Mohr, C.M., Jr. and Newman, J., Mass transfer to a rotating disk in transition flow, *J. Electrochem. Soc.*, 1976, vol. 123. p. 1687.
14. Law, C.G., Jr., Pierini, P., and Newman, J., Mass transfer to rotating disks and rotating rings in laminar, transition, and fully-developed turbulent flow, *Int. J. Heat Mass Transfer*, 1981, vol. 24, p. 909.
15. Law, C.G., Jr. and Newman, J., Corrosion of a rotating iron disk in laminar, transition, and fully developed turbulent flow, *J. Electrochem. Soc.*, 1986, vol. 133, p. 37.
16. Wasan, D.T., Tien, C.L., and Wilke, C.R., Theoretical correlation of velocity and eddy viscosity for flow close to a pipe wall, *AIChE J.,* 1963, vol. 9, p. 567.
17. Newman, J., Eddy diffusivity in the viscous sublayer, *Russ. J. Elecrochem.*, 2019, vol. 55, p. 1031.
18. Martem'yanov, S.A., Vorotyntsev, M.A., and Grafov, B.M., Functional form of the turbulent diffusion coefficient in the layer next to the electrode, *Sov. Electrochem.*, 1979, vol. 15, no. 6, p. 790.
19. Vorotyntsev, M.A., Martem'yanov, S.A., and Grafov, B.M., Closed equation of turbulent heat and mass transfer, *J. Exp. Theor. Phys.*, 1980, vol. 52, p. 909.
20. Martemianov, S.A., Statistical theory of turbulent mass transfer in electrochemical systems, *Russ. J. Electrochem.*, 2017, vol. 53, p. 1076.
21. Martem'yanov, S.A., Vorotyntsev, M.A., and Grafov, B.M., Derivation of the nonlocal transport equation of matter in the turbulent diffusion layer, *Sov. Electrochem.*, 1979, vol. 15, no. 6, p. 787.